Reaction between Criegee intermediates and hydroxyacetonitrile: Reaction mechanisms, kinetics, and atmospheric implications

Chaolu Xie¹ Shunyu Li² Bo Long*1,2

10

Correspondence to: Bo Long (wwwltcommon@sina.com)

Abstract. Hydroxyacetonitrile (HOCH₂CN) is released from wildfires and bleach cleaning environments, which is harmful to the environment and human health. However, its atmospheric lifetime remains unclear. Here, we theoretically investigate the reactions of Criegee intermediates (CH₂OO and *syn*-CH₃CHOO) with HOCH₂CN to explore their reaction mechanisms and obtain their quantitative kinetics. Specifically, we employ computational strategies approaching CCSDT(Q)/CBS accuracy, combined with a dual-level strategy, to unravel the key factors governing the reaction kinetics. We find an unprecedentedly low enthalpy of activation of −5.61 kcal/mol at 0 K for CH₂OO + HOCH₂CN among CH₂OO reaction with atmospheric species containing a C≡N group. Furthermore, we also find that the low enthalpy of activation is caused by hydrogen bonding interactions. Moreover, the present findings reveal the rate constant of CH₂OO + HOCH₂CN determined by loose and tight transition states has a significantly negative temperature dependence, reaching 10⁻¹⁰ cm³ molecule⁻¹ s⁻¹ close to the collisional limit at below 220 K. In addition, our findings also reveal that the rate constant of CH₂OO + HOCH₂CN is 10³-10² times faster than that of OH + HOCH₂CN below 260 K. The calculated kinetics in combination with data based on global atmospheric chemical transport model suggest that the CH₂OO + HOCH₂CN reaction dominates over the sink of HOCH₂CN at southeast China, northern India at 1 km and in the Indonesian and Malaysian regions at 5 and 10 km. The present findings also reveal that the CH₂OO + HOCH₂CN reaction leads to the formation of glycolamide, which could contribution to the formation of secondary organic aerosols.

¹ College of Physics and Mechatronic Engineering, Guizhou Minzu University, Guiyang 550025, China.

²College of Materials Science and Engineering, Guizhou Minzu University, Guiyang 550025, China

^{*}corresponding author, E-mail: wwwltcommon@sina.com (Bo Long)

1 Introduction

35

40

45

Hydroxyacetonitrile (HOCH₂CN), a reactive nitrogen-containing compound, has recently been identified as a C₂H₃NO isomer. Earlier field measurements had attributed the C₂H₃NO signal to methyl isocyanate (CH₃NCO) when using chemical ionization mass spectrometry (CIMS) (Priestley et al., 2018; Mattila et al., 2020; Wang et al., 2022a), as CIMS is insensitive to the detection of isomers, and thus cannot differentiate between the isomers of CH₃NCO and HOCH₂CN. However, very recent detection with I⁻ chemical ionization mass spectrometry (I-CIMS) identified the C₂H₃NO signal as HOCH₂CN (Finewax et al., 2024). In other words, the CH₃NCO detected in the atmosphere is essentially HOCH₂CN. Therefore, the atmospheric sources of CH₃NCO from previous investigations are actually the sources of HOCH₂CN. Consequently, HOCH₂CN is emitted in chemicals released from biomass burning, such as wildfires and agricultural fires, as well as in bleach cleaning environments (Mattila et al., 2020; Priestley et al., 2018; Wang et al., 2022a; Koss et al., 2018; Papanastasiou et al., 2020).

Previous studies have demonstrated that HOCH₂CN is secondary pollutant with negative impacts on the environment and human health (Worthy, 1985; Etz et al., 2024; Zhang et al., 2025). Specifically, smoke with HOCH₂CN can be injected into the stratosphere through pyrocumulonimbus clouds, altering the composition of stratospheric aerosols, depleting the ozone layer, and affecting the Earth's radiation balance (Bernath et al., 2022; Ma et al.; Katich et al., 2023). Additionally, HOCH₂CN is harmful to human health, including damage to the respiratory system and skin (Ganguly et al., 2017; Bucher, 1987). Therefore, understanding the chemical processes of HOCH₂CN is important in the atmosphere.

The atmospheric lifetimes of HOCH₂CN in the gas phase are not well understood. Hydroxyl radical (OH) is the most prevalent oxidant in the atmosphere (Wang et al., 2021). The generally considered removal for this species is through the reaction with hydroxyl radical (OH). However, the rate constant of OH + HOCH₂CN is very slow, about 2.6 × 10⁻¹³ cm³ molecule⁻¹ s⁻¹ at 298 K (Marshall and Burkholder, 2024). This leads to that OH makes limited contribution to the sinks of HOCH₂CN in the atmosphere. Therefore, it is necessary to explore the other removal routes for HOCH₂CN in the atmosphere.

Criegee intermediates are crucial compounds, resulting from the ozonolysis of unsaturated compounds in the atmosphere (Criegee, 1975; Osborn and Taatjes, 2015; Chhantyal-Pun et al., 2020a; Bunnelle, 1991; Chhantyal-Pun et al., 2020b). They play key roles in the chemical processes of atmosphere because they significantly contribute to the formation of hydroxyl radical (OH) and sulfuric acid during the nighttime (Novelli et al., 2014; Lester and Klippenstein, 2018; Kroll et al., 2002; Newland et al., 2018; Kukui et al., 2021). Additionally, they can form secondary organic aerosols via the formation of low-volatile organic compound percussors (Khan et al., 2018; Inomata et al., 2014; Docherty et al., 2005; Chhantyal-Pun et al., 2018). In particular, Criegee intermediates can initiate atmospheric reactions, resulting in additional sinks for atmospheric species such as the reactions of Criegee intermediates with formic acid, nitric acid, hydrochloric acid, and formaldehyde and so on (Khan et al., 2018; Peltola et al., 2020; Long et al., 2009; Chung et al., 2019; Foreman et al.,

2016; Luo et al., 2023). While reaction kinetics of Criegee intermediates with HOCH₂CN are prerequisite for elucidating its chemical processes and finding new sink pathways in the atmosphere, its kinetics are unknown.

In this article, we have investigated the reactions of Criegee intermediates (CH₂OO and *syn*-CH₃CHOO) with HOCH₂CN by using specific computational strategies and methods to obtain quantitative enthalpies of activation at 0 K for R1 and R2 (See Scheme 1). Then, we used a dual-level strategy to obtain their quantitative rate constants under atmospheric conditions. In our dual-level strategy, W3X-L//DF-CCSD(T)-F12b/jun-cc-pVDZ is used to obtain conventional transition state theory rate constants, while validated DFT methods capture recrossing and tunnelling effects through CVT with small-curvature tunnelling. Additionally, torsional anharmonicity and anharmonicity are considered in kinetics calculations. We also considered the decomposition process of the intermediate product formed in R1. Finally, we discuss the importance of these reactions investigated here by comparing with the corresponding OH radical reactions combined with the atmospheric concentrations of these species based on global atmospheric chemistry transport model GEOS-Chem (http://www.geoschem.org).

$$HOCH_2CN + CH_2OO$$

$$\xrightarrow{TS1} HO$$
 C
 CH_2
 CH_2

$$HOCH_2CN + syn\text{-}CH_3CHOO \xrightarrow{\text{s-TS1}} HO \xrightarrow{\text{C}} CH_3 \text{ (R2)}$$

Scheme 1. The reaction route for CH₂OO/syn-CH₃CHOO) + HOCH₂CN

2 Computational methods and strategies

55

60

65

75

2.1 Electronic structure methods and strategies

For simplicity, the activation enthalpy at 0 K is defined as the difference between the transition state and the reactants, abbreviated as ΔH_0^{\ddagger} . The difference between the products and the reactants is defined the reaction enthalpy at 0 K, abbreviated as ΔH_0 .

Morden quantum chemical methods and reaction rate theory can be used to obtain quantitative kinetics for atmosphere reactions (Long et al., 2018). However, the calculated processes are very complex, where error bars are controlled by multiple parameters. Furthermore, the parameters are correlated with each other. Gas-phase chemical reactions also crucially depend on entropies in thermalized conditions at non-zero temperatures, as well as excess energy, collisional stabilization, and fall-off effects in non-thermalized conditions. However, accurate determination of ΔH_0^{\ddagger} remains essential for calculating

quantitative kinetics. The quantitative ΔH_0^{\ddagger} that is determined by optimized geometries, zero-point vibrational energies, and single point energies in electronic structure methods (Long et al., 2019a).

80

90

95

100

Our previous investigations have shown that W3X-L (Chan and Radom, 2015)//DF-CCSD(T)-F12b/jun-cc-pVDZ (Győrffy and Werner, 2018; Parker et al., 2014) can be utilized to obtain quantitative ΔH₀[‡] for the bimolecular reactions containing Criegee intermediate (Wang et al., 2022b; Long et al., 2021; Xie et al., 2024; Zhang et al., 2024). Here, we used W3X-L//DF-CCSD(T)-F12b/jun-cc-pVDZ to investigate the CH₂OO + HOCH₂CN reaction. Additionally, CCSD(T)-F12a/cc-pVDZ-F12 was used to validate the reliability of DF-CCSD(T)-F12b/jun-cc-pVDZ for optimized geometries and calculated frequencies in the CH₂OO + HOCH₂CN reaction. Thus, with respect to *syn*-CH₃CHOO + HOCH₂CN, the validated DF-CCSD(T)-F12b/jun-cc-pVDZ method was used to do geometrical optimization and frequency calculations. In single point energy calculations, it is noted that W3X-L is equal to W2X and post-CCSD(T) components (Chan and Radom, 2015). Here, we assume that post-CCSD(T) contribution of *syn*-CH₃CHOO + HOCH₂CN approximately equates to the contribution from CH₂OO + HOCH₂CN. We used the approximation strategy mentioned previously (Sun et al., 2023) to obtain the accuracy close to W3X-L in equation (1) for *syn*-CH₃CHOO + HOCH₂CN to reduce computational costs.

$$\Delta E_{\text{BE}}^{\ddagger,s-\text{TS1}} = \Delta E_{\text{W2X}}^{\ddagger,s-\text{TS1}} + \Delta E_{\text{W3X-L-W2X}}^{\ddagger,\text{TS1}} \tag{1}$$

Here, $\Delta E_{\rm BE}^{\pm,s-{\rm TS1}}$ is the barrier height for the transition state s-TS1 (See Scheme 1). $\Delta E_{\rm W2X}^{\pm,s-{\rm TS1}}$ is the barrier height for s-TS1 calculated by W2X. $\Delta E_{\rm W3X-L-W2X}^{\pm,{\rm TS1}}$ is post-CCSD(T) contribution that comes from the difference between W3X-L and W2X in TS1 (See Fig. 1 and 2). The benchmark methods are called higher level (HL) structure methods; this helps to clearly illustrate the dual-level strategy for kinetics calculations discussed below.

A reliable density functional method was chosen in comparison to the benchmark results to perform direct kinetics calculations. Here, we chose M06-CR (Long et al., 2016)/MG3S (Zhao et al., 2005) and M11-L (Peverati and Truhlar, 2012) /MG3S functional method for the reactions of CH₂OO and *syn*-CH₃CHOO with HOCH₂CN due to the mean unsigned error (MUD) of 0.23 kcal/mol and 0.72 kcal/mol as listed in Table 1, respectively. M06CR/MG3S and M11-L/MG3S are called lower level (LL) electronic structure method in the present work. The intrinsic reaction coordinate (IRC) was performed by M11-L/MG3S, and the results were depicted the results in Figure S3.

Table 1. The enthalpies of activation at 0 K for the transition states of the CH₂OO/syn-CH₃CHOO + HOCH₂CN reactions by various theoretical methods (in kcal/mol).

Methods	ΔH_0^{\ddagger} TS1	MUD	
CH ₂ OO + HOCH ₂ CN	151		
W3X-L//DF-CCSD(T)-F12b/jun-cc-pVDZ	-5.61	0.00	
M06CR/MG3S	-5.38	0.23	
W2X//CCSD(T)-F12a/cc-pVDZ-F12	-6.16	0.55	
W2X//DF-CCSD(T)-F12b/jun-cc-pVDZ	-6.19	0.58	
CCSD(T)-F12a/cc-pVDZ-F12	-5.98	0.37	
DF-CCSD(T)-F12b/jun-cc-pVDZ	-6.77	1.16	
M11-L/MG3S	-7.52	1.91	

syn-CH ₃ CHOO + HOCH ₂ CN		
$\Delta E_{BE}^{\dagger,s-TS1}//DF-CCSD(T)-F12b/jun-cc-pVDZ$	-1.39	0.00
W2X//DF-CCSD(T)-F12b/jun-cc-pVDZ	-1.97	0.58
M11-L/MG3S	-2.11	0.72
DF-CCSD(T)-F12b/jun-cc-pVDZ	-3.13	1.74
M06-CR/MG3S	0.47	1.86

105 2.2 Scale factors for calculated frequencies

Previous studies have verified that the standard scale (See Table S1) is suitable for reactants and some transition states (Bao et al., 2016b; Zhang et al., 2017). In order to further explore the effect of anharmonicity on the zero-point vibrational energy, the calculation of the specific reaction scale factors was carried out. The results in Tables S2 and S4 show that the anharmonicity can be neglected in calculating ΔH_0^{\ddagger} . Details of the calculations can be found in previous work of Long et al (Long et al., 2023). Therefore, we used standard scale factor in this work.

2.3 Kinetics methods

110

115

120

125

The rate constants of the reaction (R1) are calculated by considering the tight and loose transition states because of its low-temperature close-to-collision-limit rate constant. Here, the loose transition state refers to the process from the reactants to the pre-reaction complexes, while the tight transition state is the process from the reactants to the products via the transition state TS1 in Figure 1. The steady state approximation based on the unified statistical theory (CUS) (Garrett and Truhlar, 1982; Bao and Truhlar, 2017; Zhang et al., 2020; Long et al., 2024) is used to calculate the total rate constant by simultaneously considering both transition states by

$$k_{CUS}(T) = \frac{k_{tight}k_{loose}}{k_{tight} + k_{loose}} \tag{1}$$

where k_{tight} was calculated by using a dual-level strategy described in detail below, while k_{loose} was calculated by variable-reaction-coordinate variational transition state theory (VRC-TST) (Zheng et al., 2008; Bao et al., 2016a; Georgievskii and Klippenstein, 2003). In VRC-TST calculation, the reaction coordinate *s* is obtained by defining the distance between one pivot point on one reactant and the other pivot point on the other, and the dividing surface is defined by the pivot point connected to each reactant. The pivot point is located in a vector at a distance d from the centre of mass (COM) of the reactants, which is chosen to minimize the reaction rate. The vector connecting the pivot point to the centre of mass of reactant and is perpendicular to the plane of the reactant. The distance *s* between the pivot points was varied between 2.6 and 10 Å in steps of 0.1 Å to find the optimum value. Simultaneously, 500 Monte Carlo sampling points were used to sample single-faceted dividing surfaces. The VRC-TST calculation were performed by minimizing the rate constant by changing the distance between two pivot points and the location of the pivot points. The VRC-TST were performed using M06-CR/MG3S

for reaction R1. However, the high-pressure-limited rate constants of the reaction (R2) were calculated only by considering tight transition state s-TS1.

The dual-level strategy has been put forward and used in previous works (Long et al., 2022; Long et al., 2018, 2019b; Xia et al., 2022; Gao et al., 2024; Long et al., 2016; Sun et al., 2023). The strategy combines the theory of conventional transition states (Glasstone et al., 1941) on the HL with the theory of canonical variational transition states (Garrett and Truhlar, 1979; Truhlar et al., 1982) on the LL and takes into account the small curvature tunnelling effect (Liu et al., 1993). In addition, the torsional anharmonicity factor is considered in our strategy (Long et al., 2023; Zhang et al., 2024; Sun et al., 2023; Li and Long, 2024; Xie et al., 2024; Jiang et al., 2025). The rate constant is given by eqn (2),

$$k = k(T)_{\text{HL}}^{\text{TST}} \kappa_{LL}^{\text{SCT}}(T) \Gamma_{LL}(T) \Gamma_{fwd,LL}^{\text{MS-T}}$$
(2)

where $k(T)_{\rm HL}^{\rm TST}$ is the rate constant without recrossing and tunneling effects calculated at HL. $\kappa_{LL}^{SCT}(T)$ and $\Gamma_{LL}(T)$ is referred to tunneling transmission coefficient and recrossing transmission coefficient calculated by LL, respectively. $F_{fwd,LL}^{\rm MS-T}$ is torsional anharmonicity factor calculated by using multi-structural method with coupled torsional potential and delocalized torsions (MS-T(CD) method) (Zheng and Truhlar, 2013; Chen et al., 2022). Three factors were calculated at the validated density functional methods at LL. The calculation each component present in equation (2) were provided in Tables S5 and S6.

2.4 Software

135

140

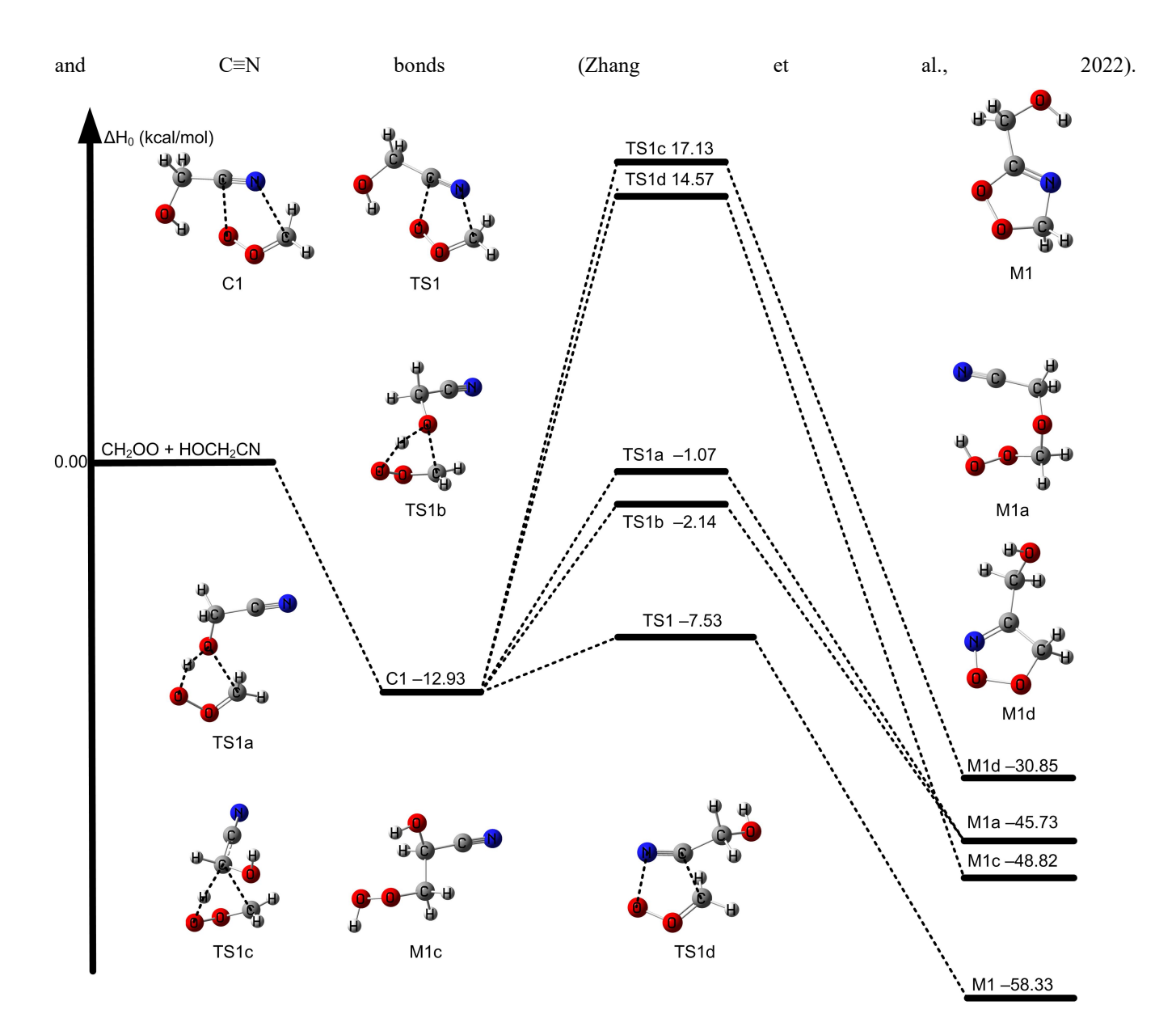
All density functional calculations were performed by using Gaussian 16 (Frisch et al., 2016) and MN-GFM (Zhao et al., 2015) for geometry optimization and frequency calculations and all coupled cluster calculations by using Molpro 2022 (Werner et al., 2012) and MRCC code (Kállay et al., 2020). Direct kinetics calculations were performed using Polyrate 2017 (Zheng et al., 2017b) and Gaussrate 2017-C (Zheng et al., 2017a). Torsional anharmonicity factor was calculated by using MSTor 2022 code (Zheng et al., 2012). And rate constants were calculated by Kisthelp program package (Canneaux et al., 2014).

3 Results and Discussion

3.1 Electronic Structure calculation results

3.1.1 The reaction of CH₂OO + HOCH₂CN

The reaction of CH₂OO + HOCH₂CN has not been reported in the literature. It is noted that there are three different functional groups (H-O, C≡N, and CH₂) in HOCH₂CN. Therefore, we explored four different mechanisms of CH₂OO + HOCH₂CN as described in Fig. 1. Three of them are similar to the CH₂OO + CH₃CN reaction, as they contain the same C-H



160 Figure 1: The relative enthalpies at 0 K for the reaction of CH₂OO + HOCH₂CN. Values are given for all species as calculated by M11-L/MG3S.

The most feasible (first) mechanism leads to the formation of five-membered cyclic intermediate M1 via $C \equiv N$ group addition to COO group in Fig. 1. Specifically, carbon atom of $C \equiv N$ group in HOCH₂CN is added to the terminal oxygen atom of CH₂OO and N atom of C $\equiv N$ group in HOCH₂CN is added to the central carbon of CH₂OO by the transition state TS1 (See Fig. 1). This mechanism is the same as CH₂OO + CH₃CN and is like that of the reaction between CH₂OO and carbonyl group (Long et al., 2021; Luo et al., 2023; Chhantyal-Pun et al., 2018; Chung et al., 2019). We called the

165

mechanism as carbon-oxygen addition coupled carbon-nitrogen addition mechanism. The second mechanism still occurs via five-membered cyclic transition states TS1a and TS1b responsible for the formation of M1a in Fig. 1. The H atom of the OH group in HOCH₂CN is migrated to the terminal oxygen atom of CH₂OO, and simultaneously the oxygen atom of OH group in HOCH₂CN is added to the central carbon atom of CH₂OO by TS1a and TS1b, which is similar to the reaction of CH₂OO with molecules containing OH group such as $H_2O/H_2O_2/HOOCH_2SCHO/CH_3C(O)OOH/HOCI$ (Long et al., 2016; Zhao et al., 2022; Long et al., 2024; Zhang et al., 2024; Xie et al., 2024). The third mechanism is the addition of C atom on the C=N group in HOCH₂CN to the central C atom of CH₂OO and the N atom of C=N group in HOCH₂CN to the terminal O of CH₂OO by TS1d. The last mechanism is that the H atom on the central CH₂ group in HOCH₂CN shifts to the terminal O atom of CH₂OO and the C atom is added to the central C atom of CH₂OO via TS1c, which leads to the formation of a peroxide. We mainly consider the most feasible mechanism in detail in this work because ΔH_0^{\ddagger} of TS1 is at least 5 kcal/mol lower than those of other reaction pathways by M11-L/MG3S (See Fig. 1). Moreover, the intermediate product M1 formed has a larger ΔH_0 of -58.33 kcal/mol in Fig.1. In addition, the calculated Gibbs free energy barriers at 298 K also show the five-ring closure reaction pathway via TS1 is the lowest in the CH₂OO + HOCH₂CN reaction (See Figure S2); this reveals that entropy has a negligible effect on reaction mechanism.

We previously showed that CCSD(T)-F12a/cc-pVDZ-F12 can reach the accuracy of CCSD(T)-F12a/cc-pVTZ-F12 for geometrical optimization and frequency calculations for reactions containing C≡N groups (Long et al., 2021; Zhang et al., 2024; Zhang et al., 2022). Therefore, we further show the reliability of DF-CCSD(T)-F12b/jun-cc-pVDZ by using CCSD(T)-F12a/cc-pVDZ-F12. As a result, the difference between W2X//CCSD(T)-F12a/cc-pVDZ-F12 and W2X//DF-CCSD(T)-F12b/jun-cc-pVDZ shows that DF-CCSD(T)-F12b/jun-cc-pVDZ is only 0.03 kcal/mol for ΔH₀[‡] of TS1 (See Table 1); this further shows that DF-CCSD(T)-F12b/jun-cc-pVDZ is quantitatively reliable for geometrical optimizations and frequency calculations in the preset investigations.

 ΔH_0^{\ddagger} of R1 via TS1 is computed to be -5.61 kcal/mol calculated by W3X-L//DF-CCSD(T)-F12b/jun-cc-pVDZ-F12, which is 5.25 lower than that of CH₂OO + CH₃CN (Zhang et al., 2022) calculated by W3X-L//CCSD(T)-F12a/cc-pVTZ-F12. The much lower ΔH_0^{\ddagger} via TS1 in R1 leads to much faster rate constant of R1, comparing with the CH₂OO + CH₃CN reaction. Simultaneously, we also found that ΔH_0^{\ddagger} of TS1 is 2.05 kcal/mol lower than that of the (CF₃)₂CFCN + CH₂OO reaction calculated using the best estimate (Jiang et al., 2025). From geometrical point of view, the much lower ΔH_0^{\ddagger} via TS1 is due to the introduction of HO group in HOCH₂CN, comparing with CH₃CN; this remarkably change the reactivity of HOCH₂CN toward CH₂OO. We note that the introduction of OH in HOCH₂CN results in the formation of hydrogen bonding in TS1. The hydrogen bonding is formed via the interaction OH group in HOCH₂CN with the terminal oxygen atom in CH₂OO in TS1. The bond distance between the hydrogen atom of HO group in HOCH₂CN and the terminal oxygen atom of CH₂OO in TS1 is computed to be 1.942 Å by DF-CCSD(T)-F12b/jun-cc-pVDZ (See Fig. 2); this shows the formation of hydrogen bonding interaction opens a way for decreasing ΔH_0^{\ddagger} .

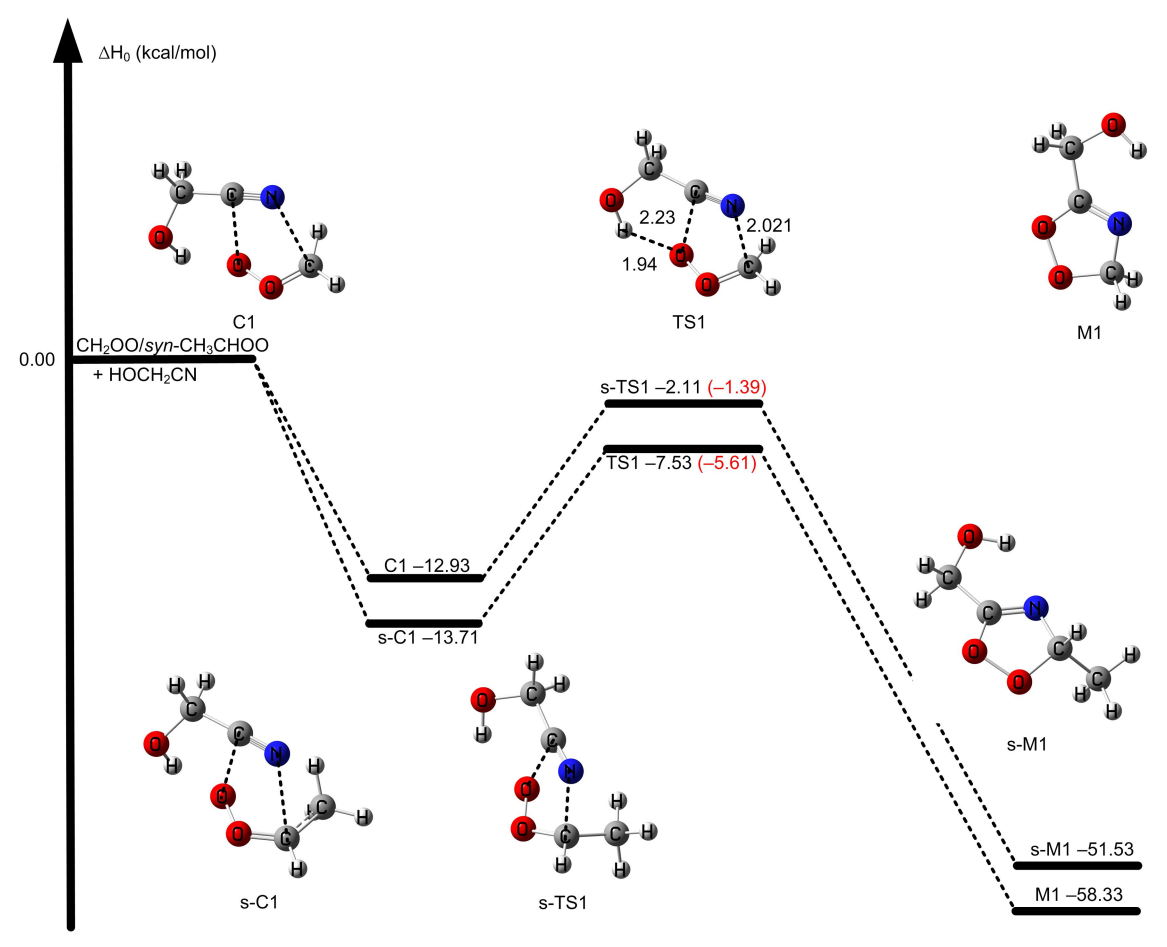


Figure 2: The relative enthalpies at 0 K for the reaction of CH₂OO/syn-CH₃CHOO + HOCH₂CN for R1 and R2. Values are given for all species as calculated by M11-L/MG3S, and in small parentheses and brackets, values are given for the transition state TS path as calculated by W3X-L//DF-CCSD(T)-F12b/jun-cc-pVDZ. The bond length in TS1 is in units of Å.

CCSD(T) has been considered as "gold standard" in the quantum chemical calculations. However, the previous investigations have shown that post-CCSD(T) is necessary to obtain quantitative reaction energy barriers for atmospheric reactions (Long et al., 2019b, 2016; Hansen et al., 2022; Xia et al., 2024). Here, we discuss the contribution of post-CCSD(T) calculations. The contribution of post-CCSD(T) is 0.58 kcal/mol from the difference between W3X-L and W2X of TS1, which is the same as the result of the reaction of CH₂OO with CH₃CN (0.58 kcal/mol) (Zhang et al., 2022) and our previous estimated value (0.50 kcal/mol) (Zhang et al., 2022; Zhao et al., 2022). This shows that post-CCSD(T) calculations are necessary for obtaining quantitative ΔH_0^{\ddagger} for the reaction of Criegee intermediate with HOCH₂CN. The MUD of M06-CR/MG3S is 0.23 kcal/mol for CH₂OO and HOCH₂CN in Table 1. Therefore, M06-CR/MG3S was chosen to perform direct kinetics calculation for the reaction of CH₂OO with HOCH₂CN.

Decomposition pathways for the formed product M1 have also been investigated at the M11-L/MG3S level; this is similar to the product decomposition pathway in the CH₂OO + CH₃CN reaction (Zhang et al., 2022). Firstly, the product M1 undergoes oxygen-oxygen bond cleavage via M1-TSa to result in forming a singlet biradical intermediate M2, which is similar to the reaction of CH₂OO + HCHO (Jalan et al., 2013). Subsequently, the intermediate M2 undergoes the formation of carbon-nitrogen bonding to form a three-member ring with ΔH_0^{\ddagger} of 21.76 kcal/mol relative to M1 via the transition state M2-TSb. Then, the three-member ring intermediate M3 then undergoes two different reaction routes. One is open-ring coupled hydrogen shift to form M4 via the transition state M3-TSc. The other is analogous to that proposed by Franzon et al. (Franzon et al., 2023), which is an open-ring coupled bond breaking to form HCHO and HOCH₂NCO via the transition state M3-TSc1. However, ΔH_0^{\ddagger} for M3-TS3c is 11.97 kcal/mol lower than that of M3-TSc1. Therefore, M3-TSc is the dominant reaction pathway for the unimolecular reaction of M3. Moreover, IRC calculations also show that M3-TSc connects well with M3 as described in Figure S3. Subsequently, the H atom of the intermediate OH on intermediate M4 is transferred to the N atom to yield the intermediate species M5. Then, the process was depicted in Fig. 3. The calculated enthalpy of reaction at 0 K of M5 is -86.55 kcal/mol, indicating the unimolecular isomerization is thermodynamically driven. Intermediate M5 undergoes unimolecular isomerization via two different pathways. In the first pathway, an intramolecular hydrogen transfer from the aldehyde group to the central carbonyl oxygen is followed by C-N bond cleavage, vielding CO and intermediate M6. Then, hydrogen shift of OH in M6 to NH group leads to the formation of glycolamide. Alternatively, a second pathway involves hydrogen migration from the aldehyde group to the central carbon atom, accompanied by C-N bond rupture, producing HNCO and glycolaldehyde. The formation of carbon monoxide proceeds with a significantly lower activation enthalpy (-54.19 kcal/mol) compared to that for glycolaldehyde (-32.32 kcal/mol), indicating that the COforming channel is kinetically favoured. Furthermore, the rate-determining step for the formation of the final product from the CH₂OO + HOCH₂CN reaction has been identified as the initial step, which is similar to the reaction of alkenes with ozone(Nguyen et al., 2015).

215

220

225

230

235

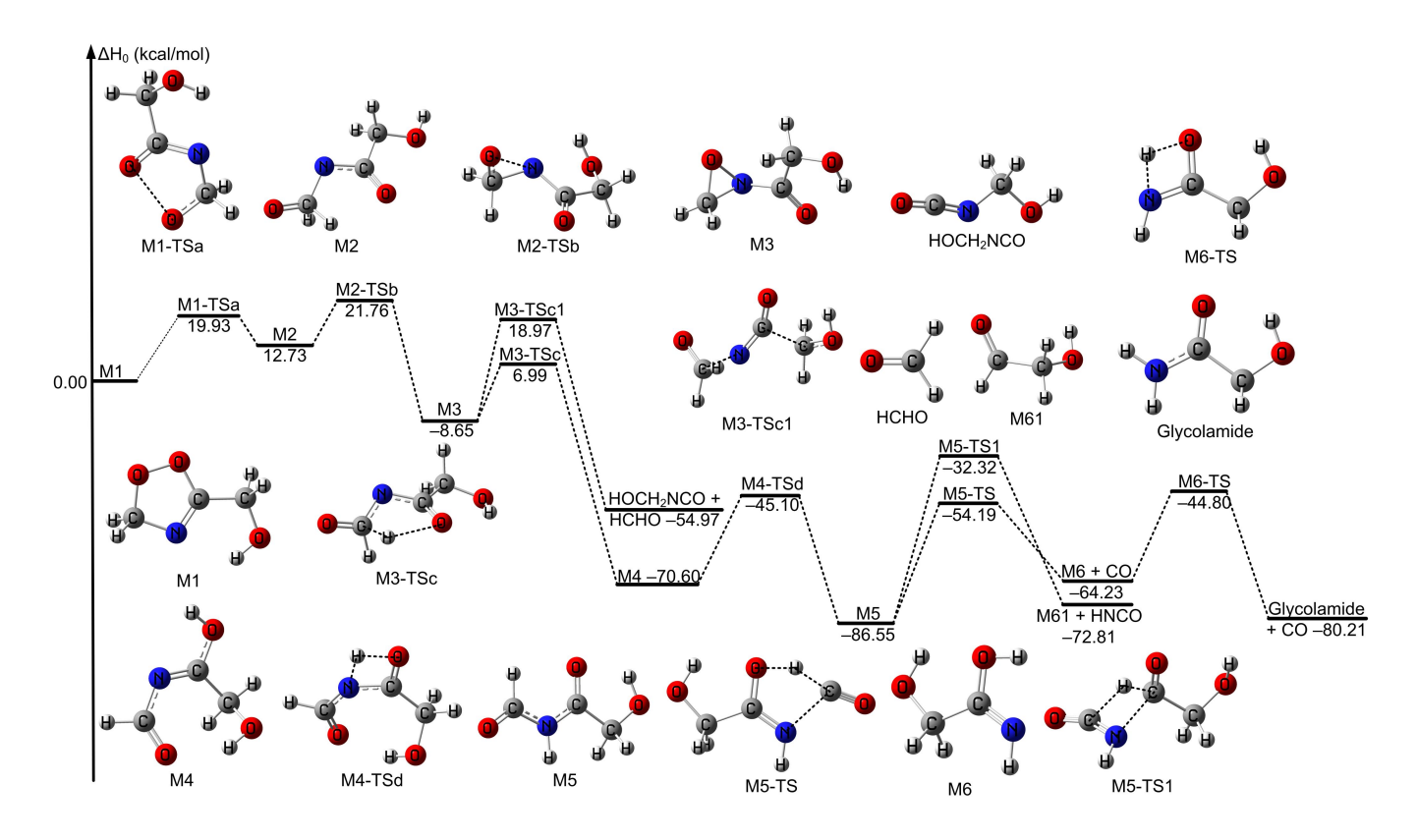


Figure 3: The relative enthalpies at 0 K for the decomposition reactions of the intermediate product M1 formed in the $CH_2OO + HOCH_2CN$ reaction. Values are given for all species as calculated by M11-L/MG3S.

240 3.1.2 The reaction of syn-CH₃CHOO + HOCH₂CN

245

250

The reaction of syn-CH₃CHOO with HOCH₂CN has been also studied by considering similar mechanisms for the reaction of CH₂OO + HOCH₂CN. The HL calculation of ΔH_0^{\ddagger} of s-TS1 was performed by employing an approximation method, as listed in eqn (1), which is discussed in method section. The lowest energy route is depicted in Fig. 2 and details can be found in Fig. S1. ΔH_0^{\ddagger} of s-TS1 is -1.39 kcal/mol calculated by HL calculation, which is 4.22 kcal/mol higher than that of TS1. The lower reactivity of syn-CH₃CHOO than CH₂OO results in the much slower reaction of syn-CH₃CHOO with HOCH₂CN. However, ΔH_0^{\ddagger} for s-TS1 is 5.45 kcal/mol is lower than the reaction of syn-CH₃CHOO + CH₃CN calculated by W3X-L//DF-CCSD(T)-F12b/jun-cc-pVDZ; this again shows that the introduction of OH group in HOCH₂CN can significantly reduce ΔH_0^{\ddagger} toward Criegee intermediates. However, the decrease in value of 5.45 kcal/mol between syn-CH₃CHOO + HOCH₂CN and syn-CH₃CHOO + CH₃CN; this indicates that the change in ΔH_0^{\ddagger} is not only determined by the change from CH₂OO to syn-CH₃CHOO. We also found that the

MUD between the HL result and M11-L/MG3S is only 0.72 kcal/mol. Therefore, the combination of M11-L functional method with MG3S basis set was chose to perform direct kinetics calculations.

3.2 Kinetics

260

265

270

275

280

The rate constants for the reaction of R1 and R2 have been calculated and listed in Table 2. The details are listed in Table S5 and S6. We have fitted the calculated rate constants by eqn (3).

$$k_{\infty} = A \left(\frac{T + T_0}{300} \right)^n \exp \left[-\frac{E(T + T_0)}{R(T^2 + T_0^2)} \right]$$
 (3)

Here, T is temperature in Kelvin and R is ideal gas constant (0.0019872 kcal mol⁻¹ K⁻¹). The fitting parameters A, n, E, and T_0 were listed in Table S7. The temperature-dependent Arrhenius activation energy have been fitted by using eqn (4) as listed in Table 3, which provides the phenomenological characteristics of temperature dependence of the rate constants.

$$E_a(T) = -R \frac{d \ln k}{d (1/T)} \tag{4}$$

The calculated rate constants for k_{R1} are decreased from 2.64 × 10⁻¹⁰ cm³ molecule⁻¹ s⁻¹ to 1.83 × 10⁻¹² cm³ molecule⁻¹ s⁻¹ at 200 - 340 K in Table 2, which shows significant negative temperature dependence. The temperature dependent activation energies are decreased from -3.45 to -5.32 kcal/mol at 200 - 340 K, which provides the evidence for the negative temperature dependence of the rate constants of R1. The rate constant for the reaction of CH₂OO + HOCH₂CN is 5.79 × 10⁻¹² cm³ molecule⁻¹ s⁻¹ at 298 K, which is 24 times larger than the rate constant for the reaction of OH + HOCH₂CN at 298 K (Marshall and Burkholder, 2024). In particular, we have found that the rate constants of reaction R1 is two magnitude order faster than the reaction of OH + HOCH₂CN when temperature below 260 K (See Table 2).

The rate constant of the reaction R2 ranges from 3.00 × 10⁻¹⁴ cm³ molecule⁻¹ s⁻¹ to 2.03 × 10⁻¹⁵ cm³ molecule⁻¹ s⁻¹ in the temperature range 200 – 340 K, which exhibits weak negative temperature dependence. As a result, we found that *syn*-CH₃CHOO make a minor contribution for the sink of HOCH₂CN because the rate constants of *syn*-CH₃CHOO + HOCH₂CN are always lower than those of the reaction of OH + HOCH₂CN at 200 – 340 K. However, the rate constant of reaction of R2 is 2.69 × 10⁻¹⁵ cm³ molecule⁻¹ s⁻¹ at 298 K, which is two orders of magnitude slower than the rate constant of the reaction of OH + HOCH₂CN and two orders of magnitude larger than that of the reaction of *syn*-CH₃CHOO + CH₃CN, suggesting that the contribution of *syn*-CH₃CHOO to the sink of HOCH₂CN is small, yet this reaction is more favourable than that for the reaction of *syn*-CH₃CHOO + CH₃CN in the atmosphere (Zhang et al., 2022). Therefore, we do not consider the contribution of *syn*-CH₃CHOO to HOCH₂CN in the atmosphere. Furthermore, for this barrierless reaction between small molecules where the torsional degrees of freedom undergo minimal change, the effects of recrossing, quantum tunnelling, and torsional anharmonicity are expected to be negligible This expectation is confirmed by our calculations, which show that the corresponding coefficients are all close to unity, as listed in Tables S5 and S6.

Table 2. The rate constants (cm³ molecule⁻¹ s⁻¹) and activation energies (kcal mol⁻¹) for the CH2OO/syn-CH3CHOO + HOCH2CN reactions at different temperatures.

T/K	l _{ro} ,	Fani	kna	Eapa	kou	$k_{\rm DJ}/k_{\rm OM}$
1/1	$\kappa_{\rm R1}$	Ea_{R1}	$\kappa_{\rm R2}$	La _{R2}	КОН	$K_{\rm R1}/K_{\rm OH}$

200	2.64×10^{-10}	-3.45	3.00×10^{-14}	-7.65	1.06×10^{-13}	2495.80
220	1.32×10^{-10}	-4.33	8.16×10^{-15}	-3.54	1.25×10^{-13}	1056.27
240	5.26×10^{-11}	-4.93	5.20×10^{-15}	-2.55	1.48×10^{-13}	354.83
250	3.39×10^{-11}	-5.14	4.46×10^{-15}	-2.33	1.61×10^{-13}	210.30
260	2.25×10^{-11}	-5.31	3.92×10^{-15}	-2.18	1.76×10^{-13}	127.83
270	1.52×10^{-11}	-5.43	3.16×10^{-15}	-2.02	1.91×10^{-13}	79.59
280	1.05×10^{-12}	-5.52	3.16×10^{-15}	-2.02	2.07×10^{-13}	50.90
298	5.79×10^{-12}	-5.59	2.69×10^{-15}	-1.98	2.39×10^{-13}	24.26
300	5.44×10^{-12}	-5.59	2.65×10^{-15}	-1.98	2.42×10^{-13}	22.45
320	3.04×10^{-12}	-5.55	2.29×10^{-15}	-1.99	2.81×10^{-13}	10.84
340	1.83×10^{-12}	-5.42	2.03×10^{-15}	-2.04	3.22×10^{-13}	5.68

3.3 Atmospheric implications

The reaction of OH with HOCH₂CN has been investigated in previous work (Marshall and Burkholder, 2024).

Therefore, we considered the competition between the R1 reaction and the OH + HOCH₂CN reaction by comparing with their rate ratios followed by eqn (5),

$$v_1 = \frac{k_{R1}[\text{CH}_2\text{OO}][\text{HOCH}_2\text{CN}]}{k_{\text{OH}}[\text{OH}][\text{HOCH}_2\text{CN}]} = \frac{k_{R1}[\text{CH}_2\text{OO}]}{k_{\text{OH}}[\text{OH}]}$$
 (5)

where k_{R1} is referred to the rate constants of the reaction of CH₂OO + HOCH₂CN, k_{OH} is rate constants of the reaction of OH with HOCH₂CN from the literature (Marshall and Burkholder, 2024).

In the atmosphere, Vereecken et al. have evaluated that the concentrations for stabilized Criegee intermediates are in the range between 10⁴ and 10⁵ molecule cm⁻³, especially in the Amazon rainforest region, where sCls could reach a maximum concentration of 10⁵ molecule cm⁻³ (Vereecken et al., 2017). Typically, the concentration of OH varies between 10⁴ and 10⁶ molecules cm⁻³ (Ren et al., 2003; Stone et al., 2012; Lelieveld et al., 2016). However, due to the consideration of reactions CH₂OO with H₂O and (H₂O)₂, the CH₂OO concentration in the GEOS-Chem model simulations is always an order of magnitude less than the results of Vereecken et al. Therefore, we consider the rate ratios between CH₂OO + HOCH₂CN and OH + HOCH₂CN at different concentrations of CH₂OO and OH at 200-340 K in Table 3, and further discuss the atmospheric implications based on global atmospheric chemistry model GEOS-Chem.

Table 3. The concentration ratio of CH₂OO to OH at different heights from different region in GEOS-Chem.

T/K	P/mbar	[CH ₂ OO] ^a	[OH] ^a	[CH ₂ OO]/[OH] ^a	$k_{\rm R1}/k_{ m OH}$	$\mathbf{v_1}^{b}$
			India			
290.2	1013	253.44	1.92×10^{4}	1.32×10^{-2}	33.27	0.44
250.5	495.9	23.10	1.40×10^{4}	1.65×10^{-3}	203.47	0.34
215.6	242.8	20.22	6.24×10^{3}	3.24×10^{-3}	1262.75	4.09
		the s	outheast of China	ļ		
290.2	1013	95.21	1.49×10^{4}	6.39×10^{-3}	33.27	0.21
250.5	495.9	19.22	1.49×10^{4}	1.29×10^{-3}	203.47	0.26
215.6	242.8	11.34	1.08×10^{4}	1.05×10^{-3}	1262.75	1.33
		Indone	sian and Malaysi	an		
290.2	1013	150.42	3.45×10^{4}	4.36×10^{-3}	33.27	0.15
250.5	495.9	79.21	1.38×10^{4}	5.74×10^{-3}	203.47	1.17
	290.2 250.5 215.6 290.2 250.5 215.6	290.2 1013 250.5 495.9 215.6 242.8 290.2 1013 250.5 495.9 215.6 242.8 290.2 1013	290.2 1013 253.44 250.5 495.9 23.10 215.6 242.8 20.22 the s 290.2 1013 95.21 250.5 495.9 19.22 215.6 242.8 11.34 Indone 290.2 1013 150.42	$\begin{array}{c ccccccccccccccccccccccccccccccccccc$	$\begin{array}{c ccccccccccccccccccccccccccccccccccc$	$\begin{array}{c ccccccccccccccccccccccccccccccccccc$

300

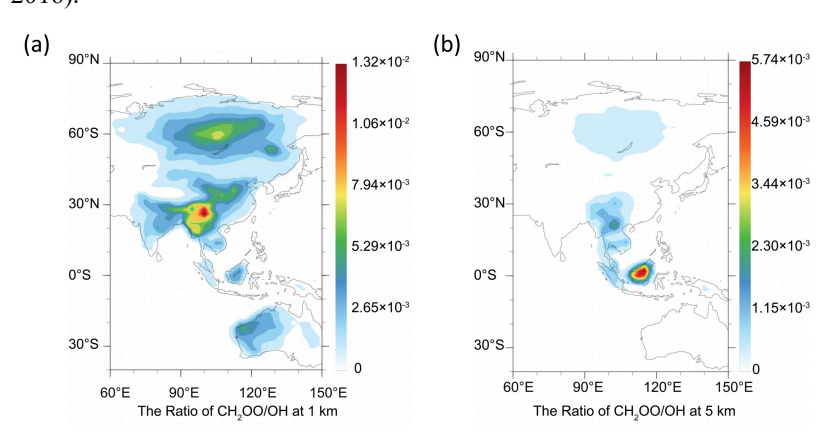
305

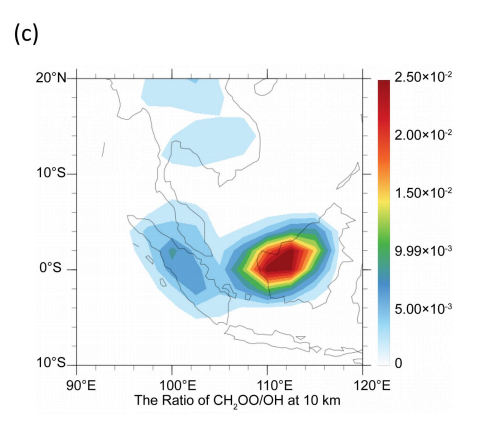
310

315

The competition between the CH₂OO + HOCH₂CN reaction and the OH + HOCH₂CN reaction is determined by two factors, one is the rate constant ratio and the other is the concentration ratio. The concentration ratio decreases with increasing altitude until two orders of magnitude are observed at 10 km in the Indonesian and Malaysian regions. It is noted that when the altitude increases, the atmospheric temperature is remarkably decreased. The atmospheric temperatures are 250.5-198 K at the altitudes from 5-15 km. The results show that although the concentration ratio of two orders of magnitude, CH₂OO does make some contribution to the sink of HOCH₂CN at 1 km. At 10 km, CH₂OO + HOCH₂CN can completely dominate over the OH + HOCH₂CN reaction in India, southeast China, Indonesia, and Malaysian region (See Table 3 and Figure 4). However, CH₂OO only dominates over the sink of HOCH₂CN in the Indonesian and Malaysian regions due to the relatively large ratio of rate constants and concentration ratios at low temperatures at 5 km. Using the model data, we find that the sink of CH₂OO to HOCH₂CN has strong geographical and sensitivity to altitude (See Fig. 4.).

The reaction products of HOCH₂CN with OH radicals exhibit significant differences from those formed by the reaction of CH₂OO with HOCH₂CN. The main products of the HOCH₂CN + OH reaction are H₂O and the HOC(H)CN radical, which subsequently reacts with O₂ to yield HO₂ and formyl cyanide (HC(O)CN) (Marshall and Burkholder, 2024). In contrast, the reaction of HOCH₂CN with CH₂OO proceeds through chemical transformation processes, ultimately forming CO and glycolamide. Glycolamide is an amide, which can contribute to the formation of secondary organic aerosols and an important interstellar molecule (Joshi and Lee, 2025; Sanz-Novo et al., 2020; Yao et al., 2016).





^a the data were extracted in the work of Long et al. (Long et al., 2024)

b the product of rate ratio and concentration ratio.

Figure 4: The ratio of CH₂OO to OH at night from literature.(Long et al., 2024) (a) at 1 km, (b) at 5 km, (c) at 10 km, (d)at 15 km.

4 Conclusions

320

325

330

335

340

345

Wildfires have attracted the attention of researchers due to their impact on aerosols and the ozone layer, which can lead to adverse effects on the environment and human health, HOCH₂CN is a harmful species present in wildfires. Thus, it is necessary to study its atmospheric chemical processes. The quantitative kinetics for reactions of Criegee intermediates with HOCH₂CN have been investigated by using specific computational strategies for electronic structure calculations and duallevel strategy for kinetics calculations coupled with atmospheric chemistry transport model analysis. The high-accuracy quantum chemical calculations were performed by using W3X-L//DF-CCSD(T)-F12b/jun-cc-pVDZ-F12 for reaction of R1 close to CCSDT(O)/CBS accuracy and an approximation strategy to reach W3X-L accuracy for R2. Additionally, CCSD(T)-F12a/cc-pVDZ-F12 was used to verified the reliability of DF-CCSD(T)-F12b/jun-cc-pVDZ-F12 for reaction R1. Four mechanisms were found for the reactions of CH2OO and HOCH2CN, with the lowest energy pathway route called carbonoxygen addition coupled carbon-nitrogen addition. We find an unprecedentedly low ΔH_0^{\dagger} of -5.61 kcal/mol for the reactions of CH₂OO with C≡N group of atmospheric species. Simultaneously, we show that the final product in the CH₂OO + HOCH₂CN reaction is glycolamide and CO, where glycolamide could contribution to the formation of secondary organic aerosols. The present findings uncover that the post-CCSD(T) is necessary to obtain quantitative ΔH_0^{\ddagger} because its contribution is 0.58 kcal/mol. However, we also find that all the factors contain anharmonicity, recrossing and tunneling, torsional anharmonicity effects, which are negligible for obtaining quantitative rate constants. The rate constants for the CH₂OO with HOCH₂CN increase from 3.18 × 10⁻¹⁰ to 2.25 × 10⁻¹¹ cm³ molecule⁻¹ s⁻¹, which is two orders of magnitude higher than the reaction of OH + HOCH₂CN below 260 K. Therefore, the reaction of CH₂OO with HOCH₂CN dominates over the sinks of HOCH₂CN in southeast China, northern India at 5 km and in the Indonesian and Malaysian regions at 5 and 10 km. This work provides a new insight into the role of Criegee intermediate in the removal of HOCH₂CN.

Supplement. The following information is provided in the Supplement: Standard scale factors and Specific Reaction Scale Factors; The activate enthalpies at 0 K for the CH₂OO + HOCH₂CN reaction at different methods; The anharmonicity effect for the enthalpy of activation; The rate constants of the reaction of R1 and R2; The fitting parameters for k₁ and k₂; The ratio of the rate constants at various temperatures and different concentration; Absolute energies (Hartree) and the Cartesian coordinates (Å) of the optimized geometries; The relative enthalpies at 0 K for the reaction of CH₂OO + HOCH₂CN.

Data availability. All raw data can be provided by the corresponding authors upon request.

Author contributions. Chaolu Xie performed the calculations, analysed and interpretation of data, and wrote the manuscript draft. Shunyu Li performed the calculations. Bo Long designed the project, analysed and interpretation of data, and reviewed and edited the manuscript.

355

Competing interests. The authors declare that they have no conflict of interest.

Acknowledgements. We also thank the Minnesota Supercomputing Institute for computational resources

Financial support. This work was supported in part by the National Natural Science Foundation of China (42120104007 and 41775125,) and by Guizhou Provincial Science and Technology Projects, China (CXTD 2022001 and GCC 2023026).

Reference

- Bao, J. L. and Truhlar, D. G.: Variational transition state theory: theoretical framework and recent developments, Chemical Society Reviews, 46, 7548-7596, 10.1039/C7CS00602K, 2017.
- Bao, J. L., Zhang, X., and Truhlar, D. G.: Barrierless association of CF₂ and dissociation of C₂F₄ by variational transition-state theory and system-specific quantum Rice–Ramsperger–Kassel theory, Proceedings of the National Academy of Sciences, 113, 13606-13611, 10.1073/pnas.1616208113, 2016a.
- Bao, J. L., Zheng, J., and Truhlar, D. G.: Kinetics of Hydrogen Radical Reactions with Toluene Including Chemical Activation Theory Employing System-Specific Quantum RRK Theory Calibrated by Variational Transition State Theory, Journal of the American Chemical Society, 138, 2690-2704, 10.1021/jacs.5b11938, 2016b.
 - Bernath, P., Boone, C., and Crouse, J.: Wildfire smoke destroys stratospheric ozone, Science, 375, 1292-1295, 10.1126/science.abm5611, 2022.
- Bucher, J. R.: Methyl isocyanate: A review of health effects research since Bhopal, Fundamental and Applied Toxicology, 9, 367-379. https://doi.org/10.1016/0272-0590(87)90019-4, 1987.
 - Bunnelle, W. H.: Preparation, properties, and reactions of carbonyl oxides, Chemical Reviews, 91, 335-362, 10.1021/cr00003a003, 1991.
 - Canneaux, S., Bohr, F., and Henon, E.: KiSThelP: A program to predict thermodynamic properties and rate constants from quantum chemistry results†, Journal of Computational Chemistry, 35, 82-93, https://doi.org/10.1002/jcc.23470, 2014.
- Chan, B. and Radom, L.: W2X and W3X-L: Cost-Effective Approximations to W2 and W4 with kJ mol-1 Accuracy, Journal of Chemical Theory and Computation, 11, 2109-2119, 10.1021/acs.jctc.5b00135, 2015.
 - Chen, W., Zhang, P., Truhlar, D. G., Zheng, J., and Xu, X.: Identification of Torsional Modes in Complex Molecules Using Redundant Internal Coordinates: The Multistructural Method with Torsional Anharmonicity with a Coupled Torsional Potential and Delocalized Torsions, Journal of Chemical Theory and Computation, 18, 7671-7682, 10.1021/acs.jctc.2c00952, 2022
- 385 2022.
 - Chhantyal-Pun, R., Khan, M. A. H., Taatjes, C. A., Percival, C. J., Orr-Ewing, A. J., and Shallcross, D. E.: Criegee intermediates: production, detection and reactivity, International Reviews in Physical Chemistry, 39, 385-424, 10.1080/0144235X.2020.1792104, 2020a.
- Chhantyal-Pun, R., Khan, M. A. H., Zachhuber, N., Percival, C. J., Shallcross, D. E., and Orr-Ewing, A. J.: Impact of Criegee Intermediate Reactions with Peroxy Radicals on Tropospheric Organic Aerosol, ACS Earth and Space Chemistry, 4, 1743-1755, 10.1021/acsearthspacechem.0c00147, 2020b.
 - Chhantyal-Pun, R., Rotavera, B., McGillen, M. R., Khan, M. A. H., Eskola, A. J., Caravan, R. L., Blacker, L., Tew, D. P., Osborn, D. L., Percival, C. J., Taatjes, C. A., Shallcross, D. E., and Orr-Ewing, A. J.: Criegee Intermediate Reactions with Carboxylic Acids: A Potential Source of Secondary Organic Aerosol in the Atmosphere, ACS Earth and Space Chemistry, 2,
- 395 833-842, 10.1021/acsearthspacechem.8b00069, 2018.
 Chung, C.-A., Su, J. W., and Lee, Y.-P.: Detailed mechanism and kinetics of the reaction of Criegee intermediate CH₂OO with HCOOH investigated via infrared identification of conformers of hydroperoxymethyl formate and formic acid anhydride, Physical Chemistry Chemical Physics, 21, 21445-21455, 10.1039/C9CP04168K, 2019.
- Criegee, R.: Mechanism of Ozonolysis, Angewandte Chemie International Edition in English, 14, 745-752, 400 https://doi.org/10.1002/anie.197507451, 1975.
- Docherty, K. S., Wu, W., Lim, Y. B., and Ziemann, P. J.: Contributions of Organic Peroxides to Secondary Aerosol Formed from Reactions of Monoterpenes with O₃, Environmental Science & Technology, 39, 4049-4059, 10.1021/es050228s, 2005. Etz, B. D., Woodley, C. M., and Shukla, M. K.: Reaction mechanisms for methyl isocyanate (CH₃NCO) gas-phase degradation, Journal of Hazardous Materials, 473, 134628, https://doi.org/10.1016/j.jhazmat.2024.134628, 2024.
- Finewax, Z., Chattopadhyay, A., Neuman, J. A., Roberts, J. M., and Burkholder, J. B.: Calibration of hydroxyacetonitrile (HOCH₂CN) and methyl isocyanate (CH₃NCO) isomers using I- chemical ionization mass spectrometry (CIMS), Atmos. Meas. Tech., 17, 6865-6873, 10.5194/amt-17-6865-2024, 2024.
 - Foreman, E. S., Kapnas, K. M., and Murray, C.: Reactions between Criegee intermediates and the inorganic acids HCl and HNO₃: Kinetics and atmospheric implications, Angewandte Chemie, 128, 10575-10578, 2016.

- 410 Franzon, L., Peltola, J., Valiev, R., Vuorio, N., Kurtén, T., and Eskola, A.: An Experimental and Master Equation Investigation of Kinetics of the CH₂OO + RCN Reactions (R = H, CH₃, C₂H₅) and Their Atmospheric Relevance, The Journal of Physical Chemistry A, 127, 477-488, 10.1021/acs.jpca.2c07073, 2023. Frisch, M. e., Trucks, G., Schlegel, H. B., Scuseria, G., Robb, M., Cheeseman, J., Scalmani, G., Barone, V., Petersson, G., and Nakatsuii, H.: Gaussian 16, 2016.
- Ganguly, B. B., Mandal, S., and Kadam, N. N.: Genotoxic and Carcinogenic Effects of Methyl Isocyanate (MIC) Reviewed on Exposed Bhopal Population and Future Perspectives for Assessment of Long-Term MIC-Effect, J. Environ. Anal. Toxicol, 7, 452, 2017.
 - Gao, Q., Shen, C., Zhang, H., Long, B., and Truhlar, D. G.: Quantitative kinetics reveal that reactions of HO₂ are a significant sink for aldehydes in the atmosphere and may initiate the formation of highly oxygenated molecules via autoxidation, Physical Chemistry Chemical Physics, 26, 16160-16174, 10.1039/D4CP00693C, 2024.
- 420 autoxidation, Physical Chemistry Chemical Physics, 26, 16160-16174, 10.1039/D4CP00693C, 2024.
 Garrett, B. C. and Truhlar, D. G.: Criterion of minimum state density in the transition state theory of bimolecular reactions, The Journal of Chemical Physics, 70, 1593-1598, 10.1063/1.437698, 1979.
 - Garrett, B. C. and Truhlar, D. G.: Canonical unified statistical model. Classical mechanical theory and applications to collinear reactions, The Journal of Chemical Physics, 76, 1853-1858, 10.1063/1.443157, 1982.
- Georgievskii, Y. and Klippenstein, S. J.: Variable reaction coordinate transition state theory: Analytic results and application to the C₂H₃+H→C₂H₄ reaction, The Journal of Chemical Physics, 118, 5442-5455, 10.1063/1.1539035, 2003.
 Glasstone, S., Laidler, K. J., and Eyring, H.: The Theory of Rate Processes: The Kinetics of Chemical Reactions, Viscosity, Diffusion and Electrochemical Phenomena, McGraw-Hill Book Company, Incorporated1941.
- Győrffy, W. and Werner, H.-J.: Analytical energy gradients for explicitly correlated wave functions. II. Explicitly correlated coupled cluster singles and doubles with perturbative triples corrections: CCSD(T)-F12, The Journal of Chemical Physics, 148, 114104, 10.1063/1.5020436, 2018.
 - Hansen, A. S., Qian, Y., Sojdak, C. A., Kozlowski, M. C., Esposito, V. J., Francisco, J. S., Klippenstein, S. J., and Lester, M. I.: Rapid Allylic 1,6 H-Atom Transfer in an Unsaturated Criegee Intermediate, Journal of the American Chemical Society, 144, 5945-5955, 10.1021/jacs.2c00055, 2022.
- Inomata, S., Sato, K., Hirokawa, J., Sakamoto, Y., Tanimoto, H., Okumura, M., Tohno, S., and Imamura, T.: Analysis of secondary organic aerosols from ozonolysis of isoprene by proton transfer reaction mass spectrometry, Atmospheric Environment, 97, 397-405, https://doi.org/10.1016/j.atmosenv.2014.03.045, 2014.
 Jalan, A., Allen, J. W., and Green, W. H.: Chemically activated formation of organic acids in reactions of the Criegee intermediate with aldehydes and ketones, Physical Chemistry Chemical Physics, 15, 16841-16852, 10.1039/C3CP52598H,
- 440 2013.

 Jiang, H., Xie, C., Liu, Y., Xiao, C., Zhang, W., Li, H., Long, B., Dong, W., Truhlar, D. G., and Yang, X.: Criegee Intermediates Significantly Reduce Atmospheric (CF₃)₂CFCN, Journal of the American Chemical Society, 147, 12263-12272, 10.1021/jacs.5c01737, 2025.
- Joshi, P. R. and Lee, Y.-P.: Identification of the HO•CHC(O)NH2 Radical Intermediate in the Reaction of H + Glycolamide in Solid Para-Hydrogen and Its Implication to the Interstellar Formation of Higher-Order Amides and Polypeptides, ACS Earth and Space Chemistry, 9, 769-781, 10.1021/acsearthspacechem.4c00409, 2025.
 - Kállay, M., Nagy, P. R., Mester, D., Rolik, Z., Samu, G., Csontos, J., Csóka, J., Szabó, P. B., Gyevi-Nagy, L., Hégely, B., Ladjánszki, I., Szegedy, L., Ladóczki, B., Petrov, K., Farkas, M., Mezei, P. D., and Ganyecz, Á.: The MRCC program system: Accurate quantum chemistry from water to proteins, The Journal of Chemical Physics, 152, 074107,
- 450 10.1063/1.5142048, 2020.

 Kar, T. and Scheiner, S.: Comparison of Cooperativity in CH···O and OH···O Hydrogen Bonds, The Journal of Physical Chemistry A, 108, 9161-9168, 10.1021/jp048546l, 2004.
 - Katich, J. M., Apel, E. C., Bourgeois, I., Brock, C. A., Bui, T. P., Campuzano-Jost, P., Commane, R., Daube, B., Dollner, M., Fromm, M., Froyd, K. D., Hills, A. J., Hornbrook, R. S., Jimenez, J. L., Kupc, A., Lamb, K. D., McKain, K., Moore, F.,
- Murphy, D. M., Nault, B. A., Peischl, J., Perring, A. E., Peterson, D. A., Ray, E. A., Rosenlof, K. H., Ryerson, T., Schill, G. P., Schroder, J. C., Weinzierl, B., Thompson, C., Williamson, C. J., Wofsy, S. C., Yu, P., and Schwarz, J. P.: Pyrocumulonimbus affect average stratospheric aerosol composition, Science, 379, 815-820, 10.1126/science.add3101, 2023. Khan, M. A. H., Percival, C. J., Caravan, R. L., Taatjes, C. A., and Shallcross, D. E.: Criegee intermediates and their impacts on the troposphere, Environmental Science: Processes & Impacts, 20, 437-453, 10.1039/C7EM00585G, 2018.

- 460 Koss, A. R., Sekimoto, K., Gilman, J. B., Selimovic, V., Coggon, M. M., Zarzana, K. J., Yuan, B., Lerner, B. M., Brown, S. S., Jimenez, J. L., Krechmer, J., Roberts, J. M., Warneke, C., Yokelson, R. J., and de Gouw, J.: Non-methane organic gas emissions from biomass burning: identification, quantification, and emission factors from PTR-ToF during the FIREX 2016 laboratory experiment, Atmos. Chem. Phys., 18, 3299-3319, 10.5194/acp-18-3299-2018, 2018.
- Kroll, J. H., Donahue, N. M., Cee, V. J., Demerjian, K. L., and Anderson, J. G.: Gas-Phase Ozonolysis of Alkenes: 465 Formation of OH from Anti Carbonyl Oxides, Journal of the American Chemical Society, 124, 8518-8519, 10.1021/ja0266060, 2002.
 - Kukui, A., Chartier, M., Wang, J., Chen, H., Dusanter, S., Sauvage, S., Michoud, V., Locoge, N., Gros, V., Bourrianne, T., Sellegri, K., and Pichon, J. M.: Role of Criegee intermediates in the formation of sulfuric acid at a Mediterranean (Cape Corsica) site under influence of biogenic emissions, Atmos. Chem. Phys., 21, 13333-13351, 10.5194/acp-21-13333-2021, 2021.
- Lelieveld, J., Gromov, S., Pozzer, A., and Taraborrelli, D.: Global tropospheric hydroxyl distribution, budget and reactivity, Atmos. Chem. Phys., 16, 12477-12493, 10.5194/acp-16-12477-2016, 2016.

470

- Lester, M. I. and Klippenstein, S. J.: Unimolecular Decay of Criegee Intermediates to OH Radical Products: Prompt and Thermal Decay Processes, Accounts of Chemical Research, 51, 978-985, 10.1021/acs.accounts.8b00077, 2018.
- Li, J. and Long, B.: Dual-level strategy for quantitative kinetics for the reaction between ethylene and hydroxyl radical, The Journal of Chemical Physics, 160, 174301, 10.1063/5.0200107, 2024.
 Liu, Y. P., Lynch, G. C., Truong, T. N., Lu, D. H., Truhlar, D. G., and Garrett, B. C.: Molecular modeling of the kinetic isotope effect for the [1,5]-sigmatropic rearrangement of cis-1,3-pentadiene, Journal of the American Chemical Society, 115, 2408-2415, 10.1021/ja00059a041, 1993.
- 480 Long, B., Bao, J. L., and Truhlar, D. G.: Atmospheric Chemistry of Criegee Intermediates: Unimolecular Reactions and Reactions with Water, Journal of the American Chemical Society, 138, 14409-14422, 10.1021/jacs.6b08655, 2016. Long, B., Bao, J. L., and Truhlar, D. G.: Unimolecular reaction of acetone oxide and its reaction with water in the atmosphere, Proceedings of the National Academy of Sciences, 115, 6135-6140, 10.1073/pnas.1804453115, 2018.
- Long, B., Bao, J. L., and Truhlar, D. G.: Kinetics of the Strongly Correlated CH₃O + O₂ Reaction: The Importance of Quadruple Excitations in Atmospheric and Combustion Chemistry, Journal of the American Chemical Society, 141, 611-617, 10.1021/jacs.8b11766, 2019a.
 - Long, B., Bao, J. L., and Truhlar, D. G.: Rapid unimolecular reaction of stabilized Criegee intermediates and implications for atmospheric chemistry, Nature Communications, 10, 2003, 10.1038/s41467-019-09948-7, 2019b.
- Long, B., Xia, Y., and Truhlar, D. G.: Quantitative Kinetics of HO₂ Reactions with Aldehydes in the Atmosphere: High-490 Order Dynamic Correlation, Anharmonicity, and Falloff Effects Are All Important, Journal of the American Chemical Society, 144, 19910-19920, 10.1021/jacs.2c07994, 2022.
 - Long, B., Cheng, J.-R., Tan, X.-f., and Zhang, W.-j.: Theoretical study on the detailed reaction mechanisms of carbonyl oxide with formic acid, Journal of Molecular Structure: THEOCHEM, 916, 159-167, https://doi.org/10.1016/j.theochem.2009.09.028, 2009.
- 495 Long, B., Xia, Y., Zhang, Y.-Q., and Truhlar, D. G.: Kinetics of Sulfur Trioxide Reaction with Water Vapor to Form Atmospheric Sulfuric Acid, Journal of the American Chemical Society, 145, 19866-19876, 10.1021/jacs.3c06032, 2023. Long, B., Zhang, Y.-Q., Xie, C.-L., Tan, X.-F., and Truhlar, D. G.: Reaction of Carbonyl Oxide with Hydroperoxymethyl Thioformate: Quantitative Kinetics and Atmospheric Implications, Research, 7, 0525, 10.34133/research.0525, 2024.
- Long, B., Wang, Y., Xia, Y., He, X., Bao, J. L., and Truhlar, D. G.: Atmospheric Kinetics: Bimolecular Reactions of Carbonyl Oxide by a Triple-Level Strategy, Journal of the American Chemical Society, 143, 8402-8413, 10.1021/jacs.1c02029, 2021.
 - Luo, P.-L., Chen, I. Y., Khan, M. A. H., and Shallcross, D. E.: Direct gas-phase formation of formic acid through reaction of Criegee intermediates with formaldehyde, Communications Chemistry, 6, 130, 10.1038/s42004-023-00933-2, 2023.
- Ma, C., Su, H., Lelieveld, J., Randel, W., Yu, P., Andreae, M. O., and Cheng, Y.: Smoke-charged vortex doubles hemispheric aerosol in the middle stratosphere and buffers ozone depletion, Science Advances, 10, eadn3657, 10.1126/sciadv.adn3657,
 - Marshall, P. and Burkholder, J. B.: Kinetics and Thermochemistry of Hydroxyacetonitrile (HOCH₂CN) and Its Reaction with Hydroxyl Radical, ACS Earth and Space Chemistry, 8, 1933-1941, 10.1021/acsearthspacechem.4c00176, 2024.

- Mattila, J. M., Arata, C., Wang, C., Katz, E. F., Abeleira, A., Zhou, Y., Zhou, S., Goldstein, A. H., Abbatt, J. P. D., DeCarlo, P. F., and Farmer, D. K.: Dark Chemistry during Bleach Cleaning Enhances Oxidation of Organics and Secondary Organic Aerosol Production Indoors, Environmental Science & Technology Letters, 7, 795-801, 10.1021/acs.estlett.0c00573, 2020. Newland, M. J., Rickard, A. R., Sherwen, T., Evans, M. J., Vereecken, L., Muñoz, A., Ródenas, M., and Bloss, W. J.: The atmospheric impacts of monoterpene ozonolysis on global stabilised Criegee intermediate budgets and SO₂ oxidation: experiment, theory and modelling, Atmos. Chem. Phys., 18, 6095-6120, 10.5194/acp-18-6095-2018, 2018.
- Nguyen, T. L., Lee, H., Matthews, D. A., McCarthy, M. C., and Stanton, J. F.: Stabilization of the Simplest Criegee Intermediate from the Reaction between Ozone and Ethylene: A High-Level Quantum Chemical and Kinetic Analysis of Ozonolysis, The Journal of Physical Chemistry A, 119, 5524-5533, 10.1021/acs.jpca.5b02088, 2015.
 Nevelli A. Verenelen, L. Lelieveld, L. and Horder, H.: Direct chemistry of OH formation from stabilized Criegee.
 - Novelli, A., Vereecken, L., Lelieveld, J., and Harder, H.: Direct observation of OH formation from stabilised Criegee intermediates, Physical Chemistry Chemical Physics, 16, 19941-19951, 10.1039/C4CP02719A, 2014.
- Osborn, D. L. and Taatjes, C. A. J. I. R. i. P. C.: The physical chemistry of Criegee intermediates in the gas phase, 34, 309-360, 2015.
 Papanastasiou, D. K., Bernard, F., and Burkholder, J. B.: Atmospheric Fate of Methyl Isocyanate, CH₃NCO: OH and Cl Reaction Kinetics and Identification of Formyl Isocyanate, HC(O)NCO, ACS Earth and Space Chemistry, 4, 1626-1637, 10.1021/acsearthspacechem.0c00157, 2020.
- Parker, T. M., Burns, L. A., Parrish, R. M., Ryno, A. G., and Sherrill, C. D.: Levels of symmetry adapted perturbation theory (SAPT). I. Efficiency and performance for interaction energies, The Journal of Chemical Physics, 140, 094106, 10.1063/1.4867135, 2014.
 - Peltola, J., Seal, P., Inkilä, A., and Eskola, A.: Time-resolved, broadband UV-absorption spectrometry measurements of Criegee intermediate kinetics using a new photolytic precursor: unimolecular decomposition of CH₂OO and its reaction with
- formic acid, Physical Chemistry Chemical Physics, 22, 11797-11808, 10.1039/D0CP00302F, 2020.

 Peverati, R. and Truhlar, D. G.: M11-L: A Local Density Functional That Provides Improved Accuracy for Electronic Structure Calculations in Chemistry and Physics, The Journal of Physical Chemistry Letters, 3, 117-124, 10.1021/jz201525m, 2012.
- Priestley, M., Le Breton, M., Bannan, T. J., Leather, K. E., Bacak, A., Reyes-Villegas, E., De Vocht, F., Shallcross, B. M. A., Brazier, T., Anwar Khan, M., Allan, J., Shallcross, D. E., Coe, H., and Percival, C. J.: Observations of Isocyanate, Amide, Nitrate, and Nitro Compounds From an Anthropogenic Biomass Burning Event Using a ToF-CIMS, Journal of Geophysical Research: Atmospheres, 123, 7687-7704, https://doi.org/10.1002/2017JD027316, 2018.
 - Ren, X., Harder, H., Martinez, M., Lesher, R. L., Oliger, A., Simpas, J. B., Brune, W. H., Schwab, J. J., Demerjian, K. L., He, Y., Zhou, X., and Gao, H.: OH and HO₂ Chemistry in the urban atmosphere of New York City, Atmospheric Environment,
- 37, 3639-3651, https://doi.org/10.1016/S1352-2310(03)00459-X, 2003. Sanz-Novo, M., Belloche, A., Alonso, J. L., Kolesniková, L., Garrod, R. T., Mata, S., Müller, H. S. P., Menten, K. M., and Gong, Y.: Interstellar glycolamide: A comprehensive rotational study and an astronomical search in Sgr B2(N)★, A&A, 639, 2020.
 - Stone, D., Whalley, L. K., and Heard, D. E.: Tropospheric OH and HO₂ radicals: field measurements and model comparisons, Chemical Society Reviews, 41, 6348-6404, 10.1039/C2CS35140D, 2012.
- 545 Chemical Society Reviews, 41, 6348-6404, 10.1039/C2CS35140D, 2012.
 Sun, Y., Long, B., and Truhlar, D. G.: Unimolecular Reactions of E-Glycolaldehyde Oxide and Its Reactions with One and Two Water Molecules, Research, 6, 0143, 10.34133/research.0143, 2023.
 - Truhlar, D. G., Isaacson, A. D., Skodje, R. T., and Garrett, B. C.: Incorporation of quantum effects in generalized-transition-state theory, The Journal of Physical Chemistry, 86, 2252-2261, 10.1021/j100209a021, 1982.
- Vereecken, L., Novelli, A., and Taraborrelli, D.: Unimolecular decay strongly limits the atmospheric impact of Criegee intermediates, Physical Chemistry Chemical Physics, 19, 31599-31612, 10.1039/C7CP05541B, 2017.
 Wang, C., Mattila, J. M., Farmer, D. K., Arata, C., Goldstein, A. H., and Abbatt, J. P. D.: Behavior of Isocyanic Acid and Other Nitrogen-Containing Volatile Organic Compounds in The Indoor Environment, Environmental Science & Technology,
- Wang, G., Iradukunda, Y., Shi, G., Sanga, P., Niu, X., and Wu, Z.: Hydroxyl, hydroperoxyl free radicals determination methods in atmosphere and troposphere, Journal of Environmental Sciences, 99, 324-335, https://doi.org/10.1016/j.jes.2020.06.038, 2021.

56, 7598-7607, 10.1021/acs.est.1c08182, 2022a.

- Wang, P.-B., Truhlar, D. G., Xia, Y., and Long, B.: Temperature-dependent kinetics of the atmospheric reaction between CH₂OO and acetone, Physical Chemistry Chemical Physics, 24, 13066-13073, 10.1039/D2CP01118B, 2022b.
- Werner, H.-J., Knowles, P. J., Knizia, G., Manby, F. R., and Schütz, M.: Molpro: a general-purpose quantum chemistry program package, WIREs Computational Molecular Science, 2, 242-253, https://doi.org/10.1002/wcms.82, 2012. WORTHY, W.: Methyl Isocyanate: The Chemistry of a Hazard, Chemical & Engineering News Archive, 63, 27-33, 10.1021/cen-v063n006.p027, 1985.
- Xia, Y., Long, B., Liu, A., and Truhlar, D. G.: Reactions with Criegee intermediates are the dominant gas-phase sink for formyl fluoride in the atmosphere, Fundamental Research, 4, 1216-1224, https://doi.org/10.1016/j.fmre.2023.02.012, 2024. Xia, Y., Long, B., Lin, S., Teng, C., Bao, J. L., and Truhlar, D. G.: Large Pressure Effects Caused by Internal Rotation in the s-cis-syn-Acrolein Stabilized Criegee Intermediate at Tropospheric Temperature and Pressure, Journal of the American Chemical Society, 144, 4828-4838, 10.1021/jacs.1c12324, 2022.
- Xie, C.-L., Yang, H., and Long, B.: Reaction between peracetic acid and carbonyl oxide: Quantitative kinetics and insight into implications in the atmosphere, Atmospheric Environment, 341, 120928, https://doi.org/10.1016/j.atmosenv.2024.120928, 2024.
 - Yao, L., Wang, M. Y., Wang, X. K., Liu, Y. J., Chen, H. F., Zheng, J., Nie, W., Ding, A. J., Geng, F. H., Wang, D. F., Chen, J. M., Worsnop, D. R., and Wang, L.: Detection of atmospheric gaseous amines and amides by a high-resolution time-of-flight chemical ionization mass spectrometer with protonated ethanol reagent ions, Atmos. Chem. Phys., 16, 14527-14543, 10.5194/acp-16-14527-2016, 2016.
- 575 10.5194/acp-16-14527-2016, 2016.

 Zhang, H., Zhang, X., Truhlar, D. G., and Xu, X.: Nonmonotonic Temperature Dependence of the Pressure-Dependent Reaction Rate Constant and Kinetic Isotope Effect of Hydrogen Radical Reaction with Benzene Calculated by Variational Transition-State Theory, The Journal of Physical Chemistry A, 121, 9033-9044, 10.1021/acs.jpca.7b09374, 2017.
- Zhang, L., Truhlar, D. G., and Sun, S.: Association of Cl with C₂H₂ by unified variable-reaction-coordinate and reaction-path variational transition-state theory, Proceedings of the National Academy of Sciences, 117, 5610-5616, 10.1073/pnas.1920018117, 2020.
 - Zhang, Y.-Q., Francisco, J. S., and Long, B.: Rapid Atmospheric Reactions between Criegee Intermediates and Hypochlorous Acid, The Journal of Physical Chemistry A, 128, 909-917, 10.1021/acs.jpca.3c06144, 2024.
- Zhang, Y.-Q., Xia, Y., and Long, B.: Quantitative kinetics for the atmospheric reactions of Criegee intermediates with acetonitrile, Physical Chemistry Chemical Physics, 24, 24759-24766, 10.1039/D2CP02849B, 2022.
 - Zhang, Y., Xu, R., Huang, W., Ye, T., Yu, P., Yu, W., Wu, Y., Liu, Y., Yang, Z., Wen, B., Ju, K., Song, J., Abramson, M. J., Johnson, A., Capon, A., Jalaludin, B., Green, D., Lavigne, E., Johnston, F. H., Morgan, G. G., Knibbs, L. D., Zhang, Y., Marks, G., Heyworth, J., Arblaster, J., Guo, Y. L., Morawska, L., Coelho, M. S. Z. S., Saldiva, P. H. N., Matus, P., Bi, P., Hales, S., Hu, W., Phung, D., Guo, Y., and Li, S.: Respiratory risks from wildfire-specific PM2.5 across multiple countries
- and territories, Nature Sustainability, 10.1038/s41893-025-01533-9, 2025.

 Zhao, Y.-C., Long, B., and Francisco, J. S.: Quantitative Kinetics of the Reaction between CH₂OO and H₂O₂ in the Atmosphere, The Journal of Physical Chemistry A, 126, 6742-6750, 10.1021/acs.jpca.2c04408, 2022.

 Zhao, Y., Lynch, B. J., and Truhlar, D. G.: Multi-coefficient extrapolated density functional theory for thermochemistry and
- thermochemical kinetics, Physical Chemistry Chemical Physics, 7, 43-52, 10.1039/B416937A, 2005.

 Zhao, Y., Peverati, R., Yang, K., Luo, S., Yu, H., He, X., and Truhlar, D. G.: MN-GFM, version 6.7: Minnesota Gaussian Functional Module, 2015.
 - Zheng, J. and Truhlar, D. G.: Quantum Thermochemistry: Multistructural Method with Torsional Anharmonicity Based on a Coupled Torsional Potential, Journal of Chemical Theory and Computation, 9, 1356-1367, 10.1021/ct3010722, 2013.
- Zheng, J., Zhang, S., and Truhlar, D. G.: Density Functional Study of Methyl Radical Association Kinetics, The Journal of Physical Chemistry A, 112, 11509-11513, 10.1021/jp806617m, 2008.
- Zheng, J., Mielke, S. L., Clarkson, K. L., and Truhlar, D. G.: MSTor: A program for calculating partition functions, free energies, enthalpies, entropies, and heat capacities of complex molecules including torsional anharmonicity, Computer Physics Communications, 183, 1803-1812, https://doi.org/10.1016/j.cpc.2012.03.007, 2012.
- Zheng, J., Bao, J., Zhang, S., Corchado, J., Meana-Pañeda, R., Chuang, Y., Coitiño, E., Ellingson, B., and Truhlar, D. J. U. o. 605 M. M., MN: Gaussrate 17, 2017a.
- Zheng, J., Bao, J. L., Meana-Pañeda, R., Zhang, S., Lynch, B., Corchado, J., Chuang, Y., Fast, P., Hu, W., and Liu, Y. J. U. o. M., Minneapolis, MN: Polyrate-version 2017-C, 2017b.